Coordination polymers from alkaline-earth nodes and pyrazine carboxylate linkers

Tang, Y.; Cavaco Soares, A.; Ferbinteanu, M.; Gao, Y.; Rothenberg, G.; Tanase, S.

DOI
10.1039/c8dt02177e

Publication date
2018

Document Version
Final published version

Published in
Dalton Transactions

Dalton Transactions

PAPER

View Article Online
View Journal | View Issue

Cite this: *Dalton Trans.*, 2018, **47**, 10071

Coordination polymers from alkaline-earth nodes and pyrazine carboxylate linkers†

Yiwen Tang,[a] Alexandre Cavaco Soares,[a] Marilena Ferbinteanu,[b] Yuan Gao,[a] Gadi Rothenberg[a] and Stefania Tanase*[a]

Received 28th May 2018,
Accepted 2nd July 2018

DOI: 10.1039/c8dt02177e

rsc.li/dalton

A new series of alkaline-earth-metal based coordination polymers were synthesized by using a pyrazine-2,5-dicarboxylic acid (2,5-H_2pzdc) ligand under hydrothermal conditions. These compounds show a variety of structural topologies, reflecting the variable coordination geometries of the alkaline-earth ions as well as the key role of the metal precursor salts. Ca, Sr, and Ba give porous three-dimensional compounds, namely $[Ca(2,5\text{-pzdc})(H_2O)_2]\cdot H_2O$ (**1**), $[Sr(2,5\text{-pzdc})(H_2O)_4]\cdot H_2O$ (**3**), $[Ba(2,5\text{-pzdc})(H_2O)_4]\cdot 2H_2O$ (**4**) and $[Ba(2,5pzdc)(H_2O)_2]$ (**5**), that feature one-dimensional hydrophilic channels which are filled with water molecules. The Sr compound retains its structure when the lattice water molecules are removed, while the other compounds undergo a structural rearrangement. The hydrophilicity of the Sr compound combined with its high stability even in the absence of guest molecules are the key characteristics that determine its good water adsorption and proton conductivity properties.

Introduction

Building coordination polymers and metal–organic frameworks (MOFs) from alkaline-earth ions and organic ligands is much less explored as compared with MOFs built from transition metal or lanthanide ions.[1–7] This is mainly due to the unpredictable coordination numbers and flexible coordination geometries of alkaline-earth cations, as well as to their tendency to form solvated organic–inorganic ionic layers instead of MOFs.[3,8–11] These properties pose challenges to the rational design and crystallization processes of alkaline-earth coordination polymers and MOFs. However, the strong ionic character and the relative high charge of alkaline-earth ions enable the synthesis of coordination polymers and MOFs with versatile structures which have great chemical and thermal stability.[12,13] Indeed, recent studies showed important developments on designing alkaline-earth metal based MOFs for various applications, such as molecular storage and separations,[14–17] proton conductivity[18–21] and mechanochemical applications.[22]

Alkaline-earth metal ions have high affinity towards oxygen-based ligands, similar to lanthanide ions. Inspired by our recent work on lanthanide-based MOFs,[23,24] we embarked on a systematic study to understand the coordination of small polycarboxylate ligands, *e.g.* pyrazine-2,5-dicarboxylic acid (2,5-H_2pzdc), to alkaline-earth metal ions (Ca^{2+}, Sr^{2+} and Ba^{2+}). The 2,5-H_2pzdc ligand contains two distinct donor groups, namely the oxygen atoms of the carboxylic groups and the nitrogen atoms of the pyrazine ring. These enable the formation of highly hydrophilic MOFs that bind water selectively and have high thermal stability.[25] Furthermore, the coordination versatility of the 2,5-H_2pzdc ligand is expected to lead to a variety of structural topologies.[26,27] To the best of our knowledge, there are few studies reporting the ability of 2,5-H_2pzdc to form MOFs,[23–27] and this is the first one to report in detail the coordination of 2,5-H_2pzdc to alkaline-earth metal ions. There is only one study reporting the crystal structure of a Sr^{2+} compound with 2,5-H_2pzdc[28] and a few more alkaline-earth coordination polymers or MOFs containing the ligands pyrazine-2,3-dicarboxylic acid (2,3-H_2pzdc),[29–31] pyrazine-2,6-dicarboxylic acid (2,6-H_2pzdc)[32,33] and pyrazine-2,3,5,6-tetracarboxylic acid (2,3,5,6-H_4PZTC).[34–36]

Here we report on the coordination of 2,5-pzdc to alkaline-earth metal ions, providing details on the synthesis and characterization of five polymeric frameworks which contain Ca^{2+}, Sr^{2+} and Ba^{2+} as nodes. We highlight the diversity of the framework structures obtained as a function of the synthetic conditions used. Then, we discuss the physical properties associated with specific hydrophilic molecular networks, including water adsorption and proton conductivity properties.

[a]*Van 't Hoff Institute for Molecular Sciences, University of Amsterdam, Science Park 904, 1098 XH Amsterdam, The Netherlands. E-mail: s.grecea@uva.nl*
[b]*Faculty of Chemistry, Inorganic Chemistry Department, University of Bucharest, Dumbrava Rosie 23, Bucharest 020462, Romania*

†Electronic supplementary information (ESI) available. CCDC 1543807, 1543809 and 1543819–1543822. For ESI and crystallographic data in CIF or other electronic format see DOI: 10.1039/c8dt02177e

Experimental

All chemicals and solvents were purchased from commercial suppliers and used as received. The ligand, pyrazine-2,5-dicarboxylic acid (2,5-H_2pzdc) was recrystallized from hot water for single-crystal structure analysis.

Synthesis of alkaline-earth compounds

In a pressure resistant tube, 0.2 mmol of alkaline-earth metal salts, 0.2 mmol of 2,5-H_2pzdc and 20 ml of water were combined. Then the mixture solution was heated at 120 °C for 48 hours in a preheated oven (see Scheme 1 for details). After a slow cooling down, the resulting white crystalline solids were separated by gravitation filtration and washed twice with 5 ml of ethanol.

[Ca(2,5-pzdc)(H_2O)$_2$]·H_2O (1)

Compound **1** was obtained following a similar procedure as discussed above but using 20 ml mixture of *N*,*N*-dimethylmethanamide (DMF, 10 ml)/water (10 ml) as solvent. Yield: 39.1 mg (75% based on metal). IR (KBr, cm^{-1}): 3158 (br), 2122 (s), 2105 (m), 1606 (m), 1573 (m), 1488 (w), 1415 (m), 1328 (m), 1295 (m), 1194 (m), 1050 (s), 806 (m), 727 (w), 555 (w). C, H, N analysis (%): calcd C 27.66, H 3.07, N 10.76; found C 27.75, H 3.17, N 10.67.

[Ca(2,5-pzdc)(H_2O)$_4$] (2)

Yield: 44.5 mg (80% based on metal). Using $Ca(OH)_2$ in the general procedure described above, we obtained a white crystalline solid which is a mixture of the [Ca(2,5-pzdc)(H_2O)$_2$]·H_2O and [Ca(2,5-pzdc)(H_2O)$_4$] compounds. Because the single-crystals of compounds **1** and **2** have different shapes, they can easily be distinguished in the mother liquid using an optical microscope. Therefore, they can be separated for single-crystal XRD measurements. Detailed characterization was performed only for compound **1** since only this compound was obtained in pure form.

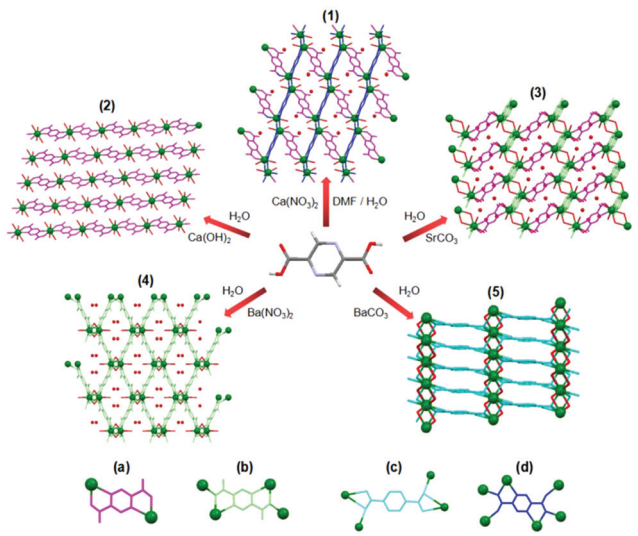

Scheme 1 Top: Synthetic routes used to crystallize various coordination polymers using alkaline-earth metal salts and 2,5-H_2pzdc. Bottom: The four different coordination modes of 2,5-pzdc linker observed within the isolated compounds. All red bonds and spheres refer to the coordinated and lattice water molecules. All hydrogen atoms within these structures are removed for clarify.

[Sr(2,5-pzdc)(H_2O)$_4$]·H_2O (3)

Yield: 50.9 mg (75% based on metal). IR (KBr, cm^{-1}): 3250 (br), 1597 (s), 1465 (m), 1384 (s), 1306 (s), 1180 (s), 1044 (s), 940 (w), 860 (w), 826 (m), 776 (s), 708 (w), 554 (s), 509 (s), 445 (s). C, H, N analysis (%): calcd C 20.99, H 3.49, N 8.16; found C 20.92, H 3.24, N 8.28.

[Ba(2,5-pzdc)(H_2O)$_4$]·2H_2O (4)

Yield: 65.2 mg (80% based on metal). Note that this compound loses the water molecules upon removing the crystals from the mother liquid, undergoing a structural change as indicated by PXRD. Elemental analysis results correspond to the composition [Ba(2,5-pzdc)] and therefore, no detailed studies were performed on this compound. IR (KBr, cm^{-1}): 3200 (br), 2035 (m), 1827 (w), 1664 (w), 1514 (m), 1441 (s), 1315 (s), 1196 (s), 1056 (s), 956 (m), 848 (s), 603 (w). C, H, N analysis (%): calcd C 25.08, H 1.04, N 9.76; found C 24.91, H 1.93, N 10.37.

[Ba(2,5-pzdc)(H_2O)$_2$] (5)

Yield: 57.1 mg (85% based on metal). IR (KBr, cm^{-1}): 3350 (br), 1613 (s), 1473 (m), 1392 (s), 1369 (w), 1301 (s), 1174 (s), 1035 (s), 956 (m), 821 (s), 775 (s), 693 (w). C, H, N analysis (%): calcd C 21.23, H 1.77, N 8.26; found C 21.53, H 2.05, N 8.27.

Physical characterization

Infrared spectra (IR, 4000–400 cm^{-1}, resol. 0.5 cm^{-1}) were recorded on a Varian 660 FTIR spectrometer equipped with a Gladi ATR device using KBr pellets as the transmission technique. Powder X-ray diffraction (PXRD) measurements were carried out on a Rigaku Miniflex X-ray diffractometer. Data were recorded from 3° to 60° with a turning speed of 2.5° per min. Thermogravimetric analysis (TGA) and differential scanning calorimetry (DSC) measurements were carried out on a STA 449 F3 Jupiter® (NETZSCH Instrument) unit. The measurements were performed under the air atmosphere with a flow of 20 ml min^{-1}. Water adsorption measurements for both the as-synthesized and dehydrated compounds **1** and **3** at 30 °C were performed in a micro-calorimeter (Calvet C80, Setaram) which can operate isothermally and is connected to a home built manometric apparatus. The dehydrated phases of compounds **1** and **3** were obtained *via* solvent evacuation under vacuum at 100 °C for 6 h.

Conductivity measurements

Samples were prepared for impedance analysis by grinding the crystalline product with a mortar and pestle to uniform particle size. Disk-shaped pellets were prepared by using a press and a die measuring 13 mm in diameter. The pellet was

placed between a pair of parallel copper plates anchored by a clamp. The typical thickness of the sample was ~0.4 mm (±0.05 mm). The electrochemical cell was then fixed with a clamp and placed in a humidity-controlled environment which is controlled by different saturated salt solutions. Impedance analysis was measured using 4-points method at different temperatures (303 K to 353 K) and various relative humidities (RH; 44% to 98%). Electrochemical impedance spectroscopy (EIS) tests were carried out under open-circuit voltage (OCV) condition using a Gamry potentiostat (Reference 600) with a frequency range of 106 Hz to 0.1 Hz and a voltage amplitude of 10 mV.

Structure determination and refinement

Single crystals of the ligand 2,5-H_2pzdc and compounds **1–5** were mounted each on a glass fiber. The crystal data have been collected on a Rigaku R-AXIS RAPID II diffractometer using graphite monochromated Mo-Kα radiation (λ = 0.71075 A) and the ω–ϕ scan technique. The structures were solved by direct methods and refined anisotropically using a full-matrix least-squares method based on F^2 with the SHELXL 97 program.[37,38] Non-hydrogen atoms were refined anisotropically. Hydrogen atoms were located and included at their calculated positions and they were refined by a riding model. The details of the crystal parameters, data collection and refinement for ligand are listed in Table S1† and for all complexes are listed in Table S2 (ESI†). CCDC 1543807, 1543809, 1543819, 1543820, 1543821, 1543822† include all supplementary crystallographic data for this paper.

Results and discussion

Crystal structure analysis

Five alkaline-earth compounds were synthesized using various alkaline-earth salts and 2,5-H_2pzdc as starting materials. This was done by varying both the type of alkaline-earth salt as well as the solvent of the reaction. Scheme 1 shows the details on reaction parameters varied and the type of the compounds obtained. Both single-crystals and polycrystalline powders were obtained in all cases. Crystallographic details are shown in Section S1 in ESI.†

During our attempts to synthesize various MOFs with alkaline-earth ions, we have also grown single crystals of the 2,5-H_2pzdc ligand in water. Fig. 1 shows its molecular crystal packing with the hydrogen bonding interactions between carboxylate groups, nitrogen atoms of the pyrazine ring and the lattice water molecules. Due to the strong hydrogen bonds established between the 2,5-H_2pzdc ligand and the crystallization water molecules, we have foreseen that water molecules might play a key role in the MOFs crystallization process. Therefore, we performed all syntheses in aqueous conditions.

Compound **1** crystallizes in the triclinic space group P_1. The asymmetric unit contains one Ca^{2+} ion, one fully deprotonated 2,5-$pzdc^{2-}$ linker, two coordinated water and one lattice water molecules. Fig. 2a shows that the Ca1 ion is coordinated to six

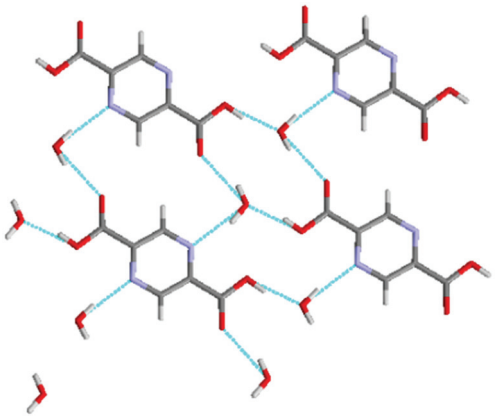

Fig. 1 The molecular structure of 2,5-H_2pzdc showing the hydrogen bonding (dash blue lines) interactions. Colour code: H, white; O, red; N, purple; C, grey.

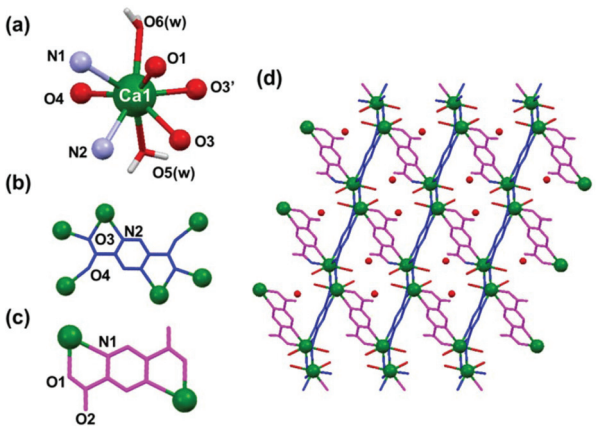

Fig. 2 (a) The coordination environment of the Ca1 ion; (b, c) The coordination modes of the 2,5-$pzdc^{2-}$ linker in **1**; (d) View of the 3D structure of **1** along *a* axis showing the 1D channels filled with water molecules. The 2,5-$pzdc^{2-}$ linkers are presented in blue and magenta, illustrating the different coordination modes. Colour code: Ca, green; O, red; N, purple; C, grey; H, white.

oxygen atoms and two nitrogen atoms to form a distorted dodecahedral coordination geometry. Four coordination sites are occupied by two different carboxylate oxygen atoms and two nitrogen atoms (O1, O3, N1 and N2) from two 2,5-$pzdc^{2-}$ linker in a chelated fashion, and the other four sites are occupied by two bridging carboxylate oxygen atoms (O3′ and O4) from two different 2,5-$pzdc^{2-}$ ligands and two oxygen atoms (O5 and O6) from two coordinated water molecules. The Ca–O bond lengths are in the range from 2.395 to 2.536 Å, and the Ca–N bond lengths are 2.575 Å and 2.647 Å, respectively. The 2,5-$pzdc^{2-}$ linkers exhibit two independent coordination modes in the molecular framework of **1**, one ligand being coordinated to six Ca^{2+} ions and the other one binding two Ca^{2+} ions (see Fig. 2b and c). The Ca1 dodecahedron in **1** is connected by two bridging carboxylate oxygen atoms to a neighbor dodecahedron to form a dinuclear unit. Then, these dinuclear

units can be viewed as a 6-connected node which is linked through 2,5-pzdc^{2-} linkers to six adjacent same units to give a three-dimensional (3D) structure. One-dimensional (1D) rhombohedral channels can be observed along the *a* direction and these channels are occupied by lattice water molecules (see Fig. 2d).

Compound **2** crystallizes as colourless needles in a monoclinic system with the space group $C2_{/c}$. Fig. 3 shows that **2** consists of Ca^{2+} ions linked by 2,5-pzdc^{2-} ligands, giving rise to a 1D chain. The asymmetric unit consists of one Ca^{2+} ion, one fully deprotonated 2,5-pzdc^{2-} ligand and four coordinated water molecules. As shown in Fig. 3a, Ca1 is surrounded by six oxygen atoms and two nitrogen atoms to adopt a distorted dodecahedral coordination geometry. Within this distorted dodecahedron, the coordination sphere of Ca1 ion contains two carboxylate oxygen atoms and two nitrogen atoms (O1, O1′, N1 and N1′) from two 2,5-pzdc^{2-} ligands in a chelated fashion as well as other four oxygen atoms (O3, O3′, O4 and O4′) from four coordinated water molecules. The Ca–O bond lengths are in the range from 2.411 to 2.539 Å, and the Ca–N bond length is 2.570 Å. Fig. 3b shows that the carboxylate groups of the fully deprotonated 2,5-pzdc^{2-} ligand in **2** have only one coordination mode. In this case, the carboxylate groups bridge one Ca^{2+} ion in a η^1 mode. The connection of the Ca^{2+} ions through bridging 2,5-pzdc^{2-} ligands leading to a 1D zig-zag chain and each chain is connected to six adjacent chains through hydrogen bonding interaction. (see Fig. 3c).

Compound **3** crystallizes in triclinic space group P_1. The asymmetric unit consists of two Sr^{2+} ions, two fully deprotonated 2,5-pzdc^{2-} linkers, eight coordinated water and two lattice water molecules. Both Sr^{2+} ions are surrounded by seven oxygen atoms and two nitrogen atoms displaying equivalent coordination spheres but with different coordination bond lengths (see Fig. 4a). In this case, both Sr1 and Sr2 are linked to two different carboxylate oxygen atoms and two nitrogen atoms (O1, O7, N1, N4) from two 2,5-pzdc^{2-} ligands in a chelated fashion as well as the third carboxylate oxygen atom (O5) from the third 2,5-pzdc^{2-} linker and four oxygen atoms (O9, O10, O11, O12) from four coordinated water molecules. The Sr1–O bond lengths range from 2.563 to 2.694 Å, while Sr2–O bond lengths range from 2.575 to 2.725 Å. The Sr1–N and Sr2–N bond lengths are 2.804, 2.810, 2.772 and 2.857 Å, respectively. Fig. 4b and c show that the 2,5-pzdc^{2-} linkers adopt two different coordination modes in **3**, one bridges four Sr^{2+} ions and the other one bridges two Sr^{2+} ion. The connection of Sr^{2+} ions through 2,5-pzdc^{2-} linkers and the hydrogen bonding interactions between coordinated water and lattice water molecules lead to a 3D structure (see Fig. 4d). The distorted hexagonal 1D channels along the *b* direction are occupied by lattice water molecules. Single-crystals of **3** can also be obtained by mixing hot aqueous solutions of $SrCO_3$ and 2,5-H_2pzdc, followed by cooling at room temperature.[28]

Compounds **4** and **5** were synthesized under the same experimental conditions but using different starting barium salts. Two different crystal structures were obtained, as confirmed by the single-crystal XRD analysis. Compound **4** crystallizes in the monoclinic space group C_2. The asymmetric unit contains one Ba^{2+} ion, one fully deprotonated 2,5-pzdc^{2-} ligand, four coordinated water and two lattice water molecules. The Ba1 ion is coordinated to eight oxygen atoms and two

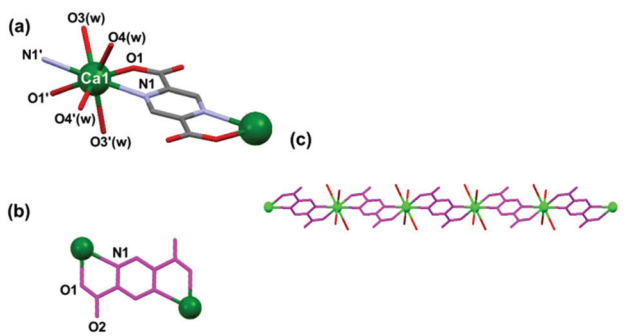

Fig. 3 (a) The coordination environment of the Ca1 ion in **2**; (b) The coordination modes of the 2,5-pzdc^{2-} linker in **2**; (c) View of the 1D chain of **2** along b axis; the lattice water molecules are removed for clarity. The 2,5-pzdc^{2-} linkers are presented in magenta, illustrating the same coordination mode. Colour code: Ca, green; O, red; N, purple; C, grey.

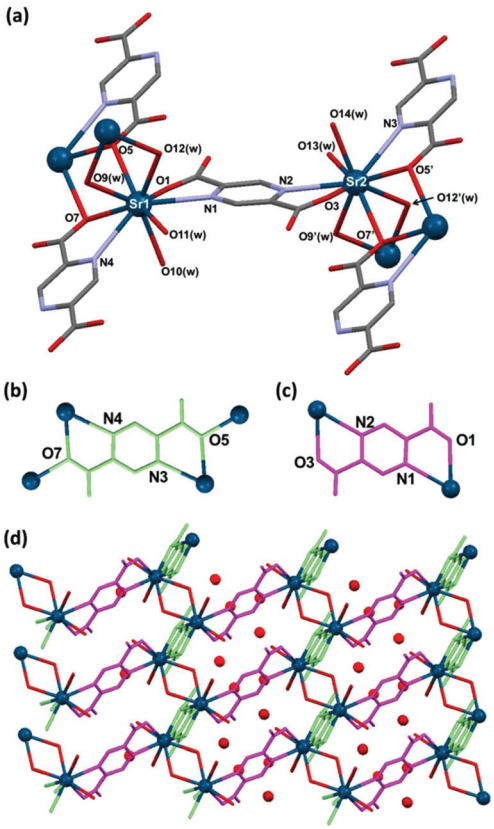

Fig. 4 (a) The coordination environments of the Sr1 and Sr2 in **3**; (b, c) the coordination modes of the 2,5-pzdc^{2-} linker in **3**; (d) view of the 3D structure of **3** along the *b* axis showing the channels filled with water molecules. The 2,5-pzdc^{2-} linkers are presented in green and magenta, illustrating the two different coordination modes. Colour code: Sr, dark blue; O, red; N, purple; C, grey.

nitrogen atoms to form its coordination sphere. The two carboxylate oxygen atoms and two nitrogen atoms (O1, O3, N1, N2) are from two 2,5-pzdc^{2-} linkers which are bound in a chelate fashion. Then, Ba1 is further coordinated by two carboxylate oxygen atoms (O1′, O3′) from two 2,5-pzdc^{2-} linkers as well as four oxygen atoms (O5, O6, O7, O8) from four coordinated water molecules (see Fig. 5a). The Ba1–O bond lengths range from 2.769 to 3.061 Å, whereas the two Ba1–N bond lengths are identical and equal to 2.90 Å. Fig. 5b shows that all 2,5-pzdc^{2-} linkers adopt one coordination mode, bridging two Ba^{2+} ions. The Ba1 polyhedron unit is linked through four μ_2–η^2 carboxylates groups and two monoatomic oxygen atoms from the coordinated water molecules to form a dinuclear Ba_2 unit. These dinuclear units are connected by 2,5-pzdc^{2-} linkers and hydrogen bonding interaction between the coordinated and lattice water molecules, leading to a 3D structure. The rhombohedral 1D channels along the *c* direction are occupied by lattice water molecules.

Unlike **4**, compound **5** crystallizes in the monoclinic space group $C2_{/c}$. The asymmetric unit of **5** has one Ba^{2+} ion, one fully deprotonated 2,5-pzdc^{2-} linker and four coordinated water molecules. Each Ba1 is bridged to ten oxygen atoms, in which four oxygen atoms (O1, O1′, O2, O2′) from two 2,5-pzdc^{2-} linkers coordinated in a chelated fashion and two oxygen atoms (O1″, O1‴) from two 2,5-pzdc^{2-} linkers bound in a monodentate mode. The other four oxygen atoms (O3, O3′, O3″, O3‴) are from four coordinated water molecules (see Fig. 6a). The Ba1–O bond lengths are in the range 2.774 to 2.993 Å. Fig. 6b shows that the carboxylate groups within 2,5-pzdc^{2-} linkers adopt one coordination mode, bridging three Ba^{2+} ions in a bridging–chelating μ_2–η^2,η^1 mode. As shown in Fig. 6c, the connection of Ba^{2+} ions through 2,5-pzdc^{2-} linkers and bridging coordinated water molecules leads **5** to a 3D structure with distorted rectangular channels along the *b* direction.

Compounds **1–5** exhibit five different crystal structures, revealing the expected versatile coordination modes of the alkaline-earth metal ions as well as the influence of the starting metal salts and the reaction conditions used. A clear trend in the connectivity of various alkaline-earth metal ions with the same linker 2,5-pzdc^{2-} can be observed in this work. Thus, the coordination number is 8 for Ca^{2+} and it increases to 10 for Ba^{2+}, reflecting the increase of the ionic radius from Ca^{2+}

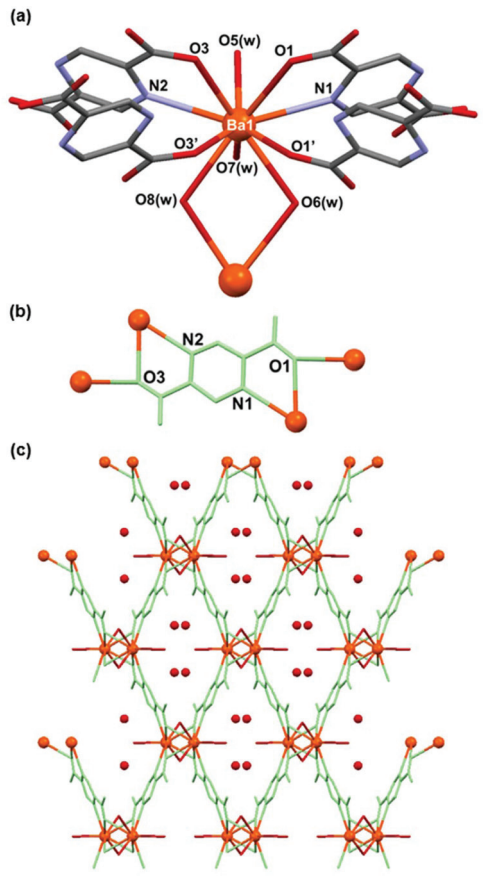

Fig. 5 (a) The coordination environment of the Ba1 ions in **4**; (b) the coordination modes of the 2,5-pzdc^{2-} ligand in **4**; (c) view of the 3D structure of **4** along the *c* axis showing the rhombohedral channels filled with water molecules. The 2,5-pzdc^{2-} linkers are presented in green, illustrating the same coordination modes. Colour code: Ba, orange; O, red; N, purple; C, grey.

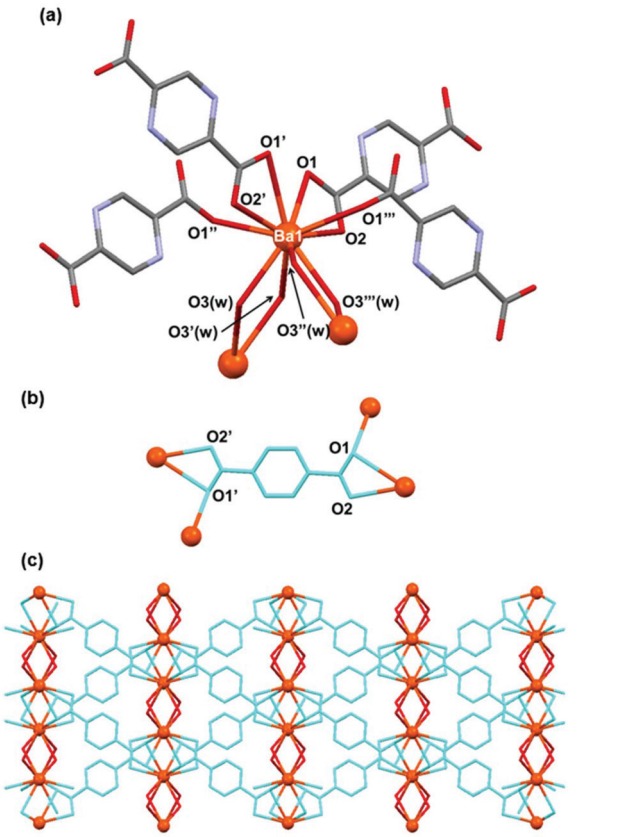

Fig. 6 (a) The coordination environment of the Ba1 ion; (b) the coordination mode of the 2,5-pzdc^{2-} linker; (c) view of the 3D structure of **5** along the *b* direction showing the empty rectangular channels. The 2,5-pzdc^{2-} linkers are presented in light blue, illustrating the same coordination modes. Colour code: Ba, orange; O, red; N, purple; C, grey.

to Ba^{2+}. This is most likely due to the decreased charge density of the alkaline-earth metal ions with larger ionic radius and their tendency to complete the coordination sphere by π-interactions with the pyrazine linker 2,5-pzdc^{2-}.[3]

The Ca^{2+} ion shows the most diverse coordination modes among the reported alkaline-earth metal based coordination compounds (see a detailed comparison in Table S3†). The coordination numbers range from 6 to 9 in different cases and the crystal structures are completely different from each other even though sometimes they bear similar or even the same ligand.[14,20,29,34,35,39–41] This behavior is likely due to the high polarizability and hygroscopic nature of the Ca^{2+} ion.[20] Other larger ions, Sr^{2+} and Ba^{2+}, have higher coordination numbers such as 8, 9 and 10, and prefer to form 3D structure built from 1D metal ion-carboxyl chains (also see Table S3†).[33,42–44] Such examples indicate that a diversity of crystal structures can be obtained by employing alkaline-earth metal ions as metal node with different, similar or even the same organic ligands as linker.

Materials characterization

The phase purity of compounds **1–5** was confirmed by comparing the experimental and simulated powder X-ray diffraction (PXRD) patterns (see Fig. 7 and S1–S5†). The results indicate that only bulk compounds **1**, **3** and **5** have a crystalline phase purity, in which all major peaks of experimental PXRD are in good agreement with the simulated ones. However, the bulk compound **2** presents a mixture phase which contains both $[Ca(2,5\text{-pzdc})(H_2O)_2]\cdot H_2O$ and $[Ca(2,5\text{-pzdc})(H_2O)_4]$, as also confirmed by single-crystal XRD studies. For the bulk compound **4**, there is a great difference between the experimental and simulated PXRD patterns, which we attribute to a crystal structure rearrangement derived from the crystal weathering effect.[16]

Based on the XRD results, we decided to perform thermogravimetric analysis (TGA) to verify the thermal stability of compounds **1**, **3** and **5**. Fig. 8 reveals that their frameworks are stable up to *ca.* 450 °C in air, decomposing above this temperature. Compounds **1** and **3** display a similar TGA curve with two steps of weight loss below 300 °C. The first weight loss step of 15 wt% (calc. 14 wt%) and 6 wt% (calc. 5 wt%) for **1** and **3** in the temperature range 75–110 °C is assigned to the removal of the lattice water and half of the coordinated water molecules for **1** as well as all lattice water molecules for **3**. The second weight loss step of 5 wt% (calc. 5 wt%) for both **1** and **3** in the temperature range of 220–260 °C corresponds to the removal of the other half of coordinated water molecules for **1** and one coordinated water molecule for **3**, respectively. However, compound **5** exhibits a different one step weight loss curve, in which 10 wt% (calc. 10 wt%) in the temperature range of 100–150 °C is assigned to the removal of all the coordinated water molecules for **5**. Based on the TGA results, we can activate these alkaline-earth based MOFs by heating to remove the guest water molecules and study further their potential applications.

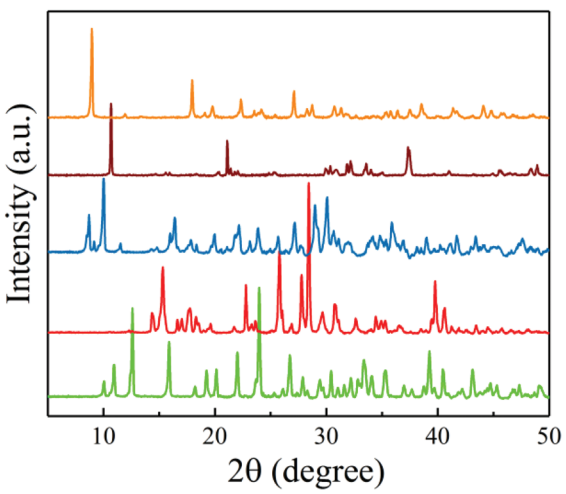

Fig. 7 PXRD patterns of the as-synthesized alkaline-earth based MOFs. Colour code: **1** (green), **2** (red), **3** (dark blue), **4** (wine) and **5** (orange).

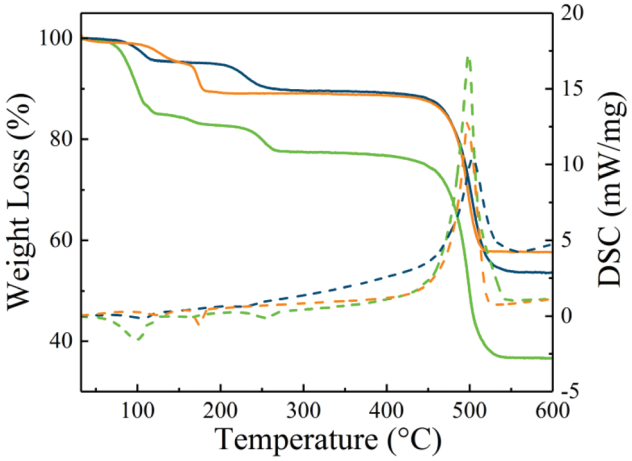

Fig. 8 TGA curves of the as-synthesized alkaline-earth based MOFs. Colour code: **1** (green), **3** (dark blue) and **5** (orange).

Therefore, we designed a suitable activation process for compounds **1** and **3** to effectively remove the lattice water molecules. Consequently, **1** and **3** were heated at both the 100 °C and 200 °C under vacuum ($<10^{-4}$ torr) for 6 h. The TGA results (see Fig. S6 and S7 in the ESI†) on the activated **1** and **3** indicate that all the lattice water molecules are removed below 100 °C. Additionally, **1** lost half of its coordinated water molecules under the same temperature. Upon activation at 200 °C, the TGA curve of **1** remains the same, whereas **3** loses some coordinated water molecules. The PXRD patterns of the activated **1** and **3** (see Fig. S1 and S3†) indicate that the coordinated water molecules play a key role in stabilising the molecular structure of these alkaline-earth compounds. A significant crystal structure change is observed upon removing the coordinated water in **1** and **3**.

Water adsorption studies

As we reported earlier, lanthanide-based MOFs constructed from 2,5-H_2pzdc linkers undergo a reversible phase change upon dehydration–rehydration procedures.[45] To investigate whether the new alkaline-earth compounds show similar be-

havior, a water adsorption study was carried out. Here we used both forms of the compounds **1** and **3**, as synthesized and activated (at 100 °C), respectively. Fig. S8† shows that the water uptake is 3.96 wt% (2.2 mmol g^{-1}) for as-synthesized **1**, indicating that 0.5 extra water molecules per Ca^{2+} metal ion can be incorporated inside the framework at saturated pressure (P/P^0 = 0.98). The extra water uptake reveals the structural flexibility of **1**, which is usually observed in molecular networks which contain metal ions with high coordination numbers.[46,47] For activated **1**, however, a very low water uptake of 0.9 wt% (0.5 mmol g^{-1}) is observed even at the saturated pressure. It is probably due to an irreversible crystal structure change derived from losing the coordinated water molecules upon activation (see Fig. S1†). The crystal structure change may cause the collapse of the 1D channels of **1**, preventing the adsorption of water molecules.[48] Additionally, the activated **1** with unsaturated coordination Ca^{2+} ions cannot return to its original structure by adsorbing water molecules (see Fig. S1†).

Fig. 9 shows that the as-synthesized **3** has a much lower water uptake, 0.9 wt% (0.5 mmol g^{-1}) below the relative pressure P/P^0 = 0.8. The water uptake reaches 2.16 wt% (1.2 mmol g^{-1}) with the water pressure increased from 0.8 to 1.0 (P/P^0). The adsorption isotherm of type V suggests that the water molecules are adsorbed in the void between particles of compound **3** as the capillary condensation occurred. The activated **3** takes up more water, about 4.8 wt% (2.6 mmol g^{-1}) at saturated pressure (P/P^0 = 0.98), reflecting that one water molecules per Sr^{2+} metal ion can be incorporated inside the channels of **3**. This shows that the activated **3** rehydrated to its original form. Compound **3** retains its original structure upon activation because no coordinated water molecules are removed (see Fig. S3†).

Proton conduction measurements

The single crystal structural study of compound **3** shows its 1D channels filled with water molecules running along the *b* axes

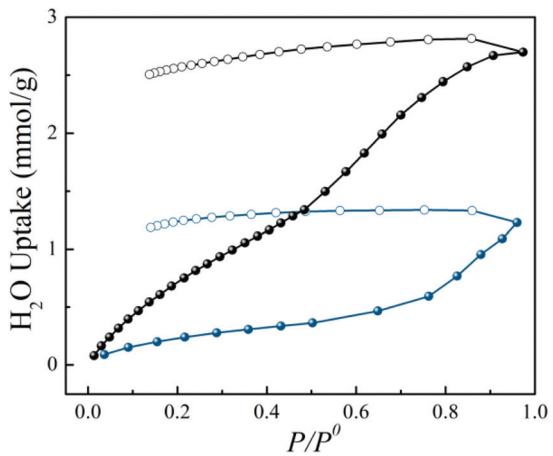

Fig. 9 Water adsorption isotherms for as-synthesized **3** (dark blue) and dehydrated **3** (black) at 30 °C. Filled and open symbols correspond to adsorption and desorption cycles, respectively.

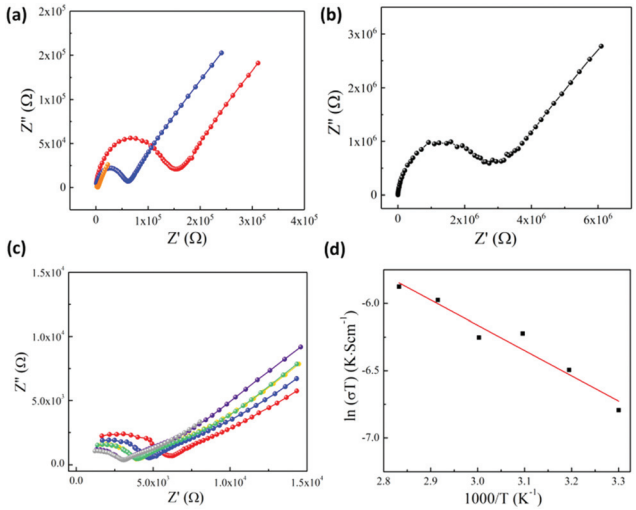

Fig. 10 (a) Impedance spectra of the dehydrated **3** at 293 K measured at 66% (red), 86% (blue) and 98% (orange) relative humidity (RH). (b) Impedance spectrum of the dehydrated **3** at 293 K at 50% RH (black). (c) Impedance spectra of the dehydrated **3** at 44% RH and 303 K (red), 313 K (blue), 323 K (yellow), 333 K (green), 343 K (purple) and 353 K (grey). (d) Arrhenius plots of the proton conductivities of dehydrated **3** at 44% RH.

(see Fig. 4d). This structural feature, in addition to the coordinated water molecules pointing toward channels, may facilitate a good proton conduction path.[49] Impedance spectra measured at different relative humidities (RH) and temperatures are shown in Fig. 10. It is worth noting that the amount of water molecules within 1D channels of compound **3** increased as the water partial pressures (RH) increased. Similar to the water adsorption, at constant temperature of 293 K, the conductivity increased from 1.12×10^{-8} to 9.05×10^{-6} S cm^{-1} when RH increased from 50% to 98%. These results indicated that the increasing of the proton conductivity has a close relationship to the amount of water molecules within 1D channels of **3**. This is due to the water molecules which can work as a proton carrier and grain boundary remover.[50] In the case of **3**, increasing the relative humidity facilitates the incorporation of water molecules into 1D channels by hydrogen bonding interactions with the carboxylate oxygen atoms, coordinated and lattice water molecules, which improve the proton conductivity.[51]

Subsequently, to understand the proton conduction mechanism mediated by the water molecule, we compared the impedance values at different temperatures, while keeping the RH at 44%. The conductivity increased from 3.70×10^{-6} to 7.95×10^{-6} S cm^{-1} with the temperature increased from 303 K to 353 K (see Fig. 10c). The proton conductivity value of **3** is comparable with that of MIL-53 and other alkaline-earth metal based MOFs (a detailed comparison is given in Table S4†). The Arrhenius activation energy of 0.16 eV is derived from these conductivity results (see Fig. 10d). This relatively low activation energy indicates that the Grotthuss mechanism is likely occuring, in which a proton hops from a proton donor to an

acceptor along a hydrogen bond.[52,53] In the case of compound **3**, the metal cations serve to improve the acidity of the coordinated water molecules, which can donate protons to adjacent lattice water molecules; therefore, protons can be transported through the hydrogen bonding networks (see Fig. S9 in ESI†).[20] However, the plausible reason behind the low proton conductivity of **3** is due to the hydrogen bonding network within the 1D channel is highly asymmetric, because the lattice water molecules are arranged as discrete clusters. This is also observed in other proton-conducting MOF materials (see Table S4†).[54,55]

Conclusions

We report here the successfully synthesis of a series of alkaline-earth coordination polymers using a pyrazine–carboxylate ligand as linker. These compounds exhibit a variety of crystal structures derived from the large and flexible coordination geometries of the alkaline-earth ions together with the coordination versatility of the 2,5-pzdc^{2-} linker used. All compounds with 3D networks feature highly hydrophilic open channels which are filled with water molecules. Notably, the Sr-based compound **3** can retain its original structure after removing all lattice water molecules from the 1D channels, thus exhibiting a potential proton conduction ability because of its appropriate pathway for proton transporting. These results suggest that it is possible to design water stable porous compounds made from abundant and non-toxic alkaline-earth metal ions.

Conflicts of interest

There are no conflicts to declare.

Acknowledgements

Y. T. and Y. G. acknowledge the China Scholarship Council (CSC) for a PhD fellowship. We thank Dr M. C. Mittelmeijer-Hazeleger (UvA) for adsorption measurements and Dr N. Yan (UvA) for feedback on the conductivity measurements. This work is part of the Research Priority Area Sustainable Chemistry of the University of Amsterdam, http://suschem.uva.nl.

Notes and references

1 T. Devic and C. Serre, *Chem. Soc. Rev.*, 2014, **43**, 6097–6115.
2 Y. Cui, B. Chen and G. Qian, *Coord. Chem. Rev.*, 2014, **273**, 76–86.
3 K. M. Fromm, *Coord. Chem. Rev.*, 2008, **252**, 856–885.
4 A. Torvisco, A. O'Brien and K. Ruhlandt-Senge, *Coord. Chem. Rev.*, 2011, **255**, 1268–1292.
5 D. Braga, F. Grepioni and O. Shemchuk, *CrystEngComm*, 2018, **16**, 2218–2227.
6 Y. Geng, P. Li, J. Li, X. Zhang, Q. Zeng and C. Wang, *Coord. Chem. Rev.*, 2017, **337**, 145–177.
7 S. Kobayashi and Y. Yamashita, *Acc. Chem. Res.*, 2011, **44**, 58–71.
8 X. Li, L. Ma, Y. Liu, L. Hou, Y. Wang and Z. Zhu, *ACS Appl. Mater. Interfaces*, 2018, **10**, 10965–10973.
9 H. I. Buvailo, V. Makhankova, V. N. Kokozay, I. Omelchenko, S. Shishkina, P. Zabierowski, D. Matoga and J. Jezierska, *Eur. J. Inorg. Chem.*, 2017, **29**, 3525–3532.
10 S. Cai, Z. He, W. Wu, F. Liu, X. Huang, S. Zheng, J. Fan and W. Zhang, *CrystEngComm*, 2017, **22**, 3003–3016.
11 P. Vishnoi, D. Kaleeswaran, A. Kalita and R. Murugavel, *CrystEngComm*, 2016, **18**, 9130–9138.
12 D. W. Lee, V. Jo and K. M. Ok, *Cryst. Growth Des.*, 2011, **11**, 2698–2701.
13 D. Saha, T. Maity and S. Koner, *Eur. J. Inorg. Chem.*, 2015, **6**, 1053–1064.
14 Y. Hou, J. Sun, D. Zhang, D. Qi and J. Jiang, *Chem. – Eur. J.*, 2016, **22**, 6345–6352.
15 D. Banerjee, Z. Zhang, A. M. Plonka, J. Li and J. B. Parise, *Cryst. Growth Des.*, 2012, **12**, 2162–2165.
16 Y. Tang, A. Kourtellaris, A. J. Tasiopoulos, S. J. Teat, D. Dubbeldam, G. Rothenberg and S. Tanase, *Inorg. Chem. Front.*, 2018, **5**, 541–549.
17 J. Cepeda, S. Pérez-YáÑez, G. Beobide, O. Castillo, E. Goikolea, F. Aguesse, L. Garrido, A. Luque and P. A. Wright, *Chem. Mater.*, 2016, **28**, 2519–2528.
18 K. Asha, M. Makkitaya, A. Sirohi, L. Yadav, G. Sheet and S. Mandal, *CrystEngComm*, 2016, **6**, 1046–1053.
19 X. Y. Dong, X. P. Hu, H. C. Yao, S. Q. Zang, H. W. Hou and T. C. W. Mak, *Inorg. Chem.*, 2014, **53**, 12050–12057.
20 A. Mallick, T. Kundu and R. Banerjee, *Chem. Commun.*, 2012, **48**, 8829–8831.
21 R. M. P. Colodrero, P. Olivera-Pastor, E. R. Losilla, D. Alonso, M. Aranda, L. Reina, J. Rius, K. Demadis, B. Moreau, D. Villemin, M. Palomino, F. Rey and A. Cabeza, *Inorg. Chem.*, 2012, **51**, 7689–7698.
22 A. Al-Terkawi, G. Scholz, F. Emmerling and E. Kemnitz, *Cryst. Growth Des.*, 2016, **4**, 1923–1933.
23 R. Plessius, R. Kromhout, A. L. Dantas Ramos, M. Ferbinteanu, M. C. Mittelmeijer-Hazeleger, R. Krishna, G. Rothenberg and S. Tanase, *Chem. – Eur. J.*, 2014, **20**, 7922–7925.
24 S. Tanase, M. C. Mittlemeijer-Hazeleger, G. Rothenberg, C. Mathonière, V. Jubera, J. M. M. Smits and R. de Gelder, *J. Mater. Chem.*, 2011, **21**, 15544–15551.
25 M. Lankelma, J. Boer, M. Ferbinteanu, A. L. D. Ramos, R. Tanasa, G. Rothenberg and S. Tanase, *Dalton Trans.*, 2015, **44**, 11380.
26 D. Ma, W. Wang, Y. Li, J. Li, C. Daiguebonne, G. Calvez and O. Guillou, *CrystEngComm*, 2010, **12**, 4372–4377.
27 B. Cai, P. Yang, J. W. Dai and J. Z. Wu, *CrystEngComm*, 2011, **13**, 985–991.
28 H. Ptasiewicz-bak and J. Leciejewicz, *J. Coord. Chem.*, 1998, **44**, 237–246.

29 S. Zhang, X. Liu, Q. Yang, Q. Wei, G. Xie and S. Chen, *CrystEngComm*, 2015, **17**, 3312.
30 Q. Yang, Y. Zhang, J. Lu, P. Xue and Z. Wang, *Acta Crystallogr.*, 2011, **67**, 1857.
31 W. Starosta and J. Leciejewicz, *J. Coord. Chem.*, 2004, **57**, 1151–1156.
32 H. Ptasiewicz-Bak and J. Leciejewicz, *J. Coord. Chem.*, 2003, **56**, 173–180.
33 H. Ptasiewicz-Bak and J. Leciejewicz, *J. Coord. Chem.*, 2003, **56**, 223–229.
34 W. Starosta and J. Leciejewicz, *J. Coord. Chem.*, 2008, **61**, 490–498.
35 S. Golafale, C. Ingram, A. Holder, W. Chen and Z. Zhang, *Inorg. Chim. Acta*, 2017, **467**, 163–168.
36 M. Gryz, W. Starosta and J. Leciejewicz, *Acta Crystallogr.*, 2005, **61**, 1920–1922.
37 *Crystal Structure 4.0: Crystal Structure Analysis Package*, Rigaku Corporation, Tokyo 196-8666, Japan.
38 SHELX97: G. M. Sheldrick, *Acta Crystallogr., Sect. A: Fundam. Crystallogr.*, 2008, **64**, 112–122.
39 L. Yang, P. Vajeeston, P. Ravindran, H. Fjellvag and M. Tilset, *Phys. Chem. Chem. Phys.*, 2011, **13**, 10191–10203.
40 X. Wang, M. Hu, J. Tian and C. Liu, *CrystEngComm*, 2016, **18**, 2864.
41 S. Chen, F. Tian, K. Huang, C. Li, J. Zhong, M. He, Z. Zhang, H. Wang, M. Du and Q. Chen, *CrystEngComm*, 2014, **16**, 7673.
42 D. Rankine, T. Keene, C. Sumby and C. Doonan, *CrystEngComm*, 2013, **15**, 9722.
43 M. Usman, C. Lee, D. Hung, S. Lee, C. Wang, T. Luo, L. Zhao, M. Wu and K. Lu, *J. Mater. Chem. C*, 2014, **2**, 3762.
44 Z. Zhang, Q. Wang, W. Li, Q. Meng and X. Zhang, *CrystEngComm*, 2012, **14**, 5042–5052.
45 Y. Gao, R. Broersen, W. Hageman, N. Yan, M. C. Mittelmeijer-Hazeleger, G. Rothenberg and S. Tanase, *J. Mater. Chem. A*, 2015, **3**, 22347–22352.
46 J. Ye, Y. Li, Y. Zhao, X. Mu, P. Zhang and Y. Wang, *CrystEngComm*, 2008, **10**, 598–604.
47 X. Wang, L. Zhang, J. Yang, F. Liu, F. Dai, R. Wang and D. Sun, *J. Mater. Chem. A*, 2015, **3**, 12777–12785.
48 Y. Lan, H. Jiang, S. Li and Q. Xu, *Adv. Mater.*, 2011, **23**, 5015–5020.
49 P. Ramaswamy, N. E. Wong and G. K. H. Shimizu, *Chem. Soc. Rev.*, 2014, **43**, 5913–5932.
50 M. Sadakiyo, T. Yamada, K. Honda, H. Matsui and H. Kitigawa, *J. Am. Chem. Soc.*, 2014, **136**, 7701–7707.
51 E. Pardo, C. Train, G. Gontard, K. Boubekeur, O. Fabelo, H. Liu, B. Dkhil, F. Lloret, K. Nakagawa, H. Tokoro, S. Ohkoshi and M. Verdaguer, *J. Am. Chem. Soc.*, 2011, **133**, 15328–15331.
52 H. R. Allcock, M. V. Phelps, E. W. Barrett, M. V. Pishko and W.-G. Koh, *Chem. Mater.*, 2006, **18**, 609.
53 T. Ogawa, T. Aonuma, T. Tamaki, H. Ohashi, H. Ushiyama, K. Yamashita and T. Yamaguchi, *Chem. Sci.*, 2014, **5**, 4878.
54 X. Y. Dong, X. P. Hu, H. C. Yao, S. Q. Zang, H. W. Hou and T. C. W. Mak, *Inorg. Chem.*, 2013, **53**, 12050.
55 T. Kundu, S. C. Sahoo and R. Banerjee, *Chem. Commun.*, 2012, **48**, 4998–5000.